Journal of Power Sources 220 (2012) 153–159

Contents lists available at SciVerse ScienceDirect

Journal of Power Sources

journal homepage: www.elsevier.com/locate/jpowsour

Conveniently fabricated heterojunction ZnO/TiO_2 electrodes using TiO_2 nanotube arrays for dye-sensitized solar cells

Rui Liu [a], Wein-Duo Yang [b,*], Liang-Sheng Qiang [a,**], Hsin-Yi Liu [b]

[a] Department of Applied Chemistry, Harbin Institute of Technology, Harbin 150001, PR China
[b] Department of Chemical and Materials Engineering, National Kaohsiung University of Applied Sciences, 415 Chien-Kung Road, Kaohsiung 807, Taiwan

HIGHLIGHTS

- We fabricate ZnO/TiO_2 heterojunction as photo-anode in DSSCs.
- We use many characterizations to investigate properties of ZnO/TiO_2 heterojunction.
- The results show that efficiency of DSSCs improves approximately double under optimum condition.

ARTICLE INFO

Article history:
Received 17 February 2012
Accepted 31 July 2012
Available online 8 August 2012

Keywords:
Titania nanotube arrays
Zinc oxide
Anodic oxidation
Electrodeposition
Dye-sensitized solar cells

ABSTRACT

TiO_2 nanotube arrays with an inner average pore diameter of 83 nm and a length of 14 μm are grown on Ti foils by electrochemical anodization in ammonium fluoride–water–glycerol solution. ZnO is introduced into the TiO_2 nanotube arrays by a convenient electrodeposition technique. ZnO/TiO_2 nanocomposites supported on Ti substrate are used as the photo-anode electrode for dye-sensitized solar cells (DSSCs). The morphology, structure and electrochemical properties are investigated using field-emission scanning electron microscopy, transmission electron microscopy, X-ray diffraction, UV–vis diffusion reflection spectroscopy, X-ray photoelectron spectroscopy and cyclic voltammetry measurements. It is found that ZnO have been embedded in the TiO_2 nanotube arrays, and changed some photoelectric properties. The conversion efficiency of the dye-sensitized solar cells is more than doubled, compared with that of bare TiO_2 nanotube arrays with deposited 60 min. This improvement comes from the synergetic effect between ZnO and TiO_2, which increases dye absorption, electron transport and electron lifetime.

1. Introduction

Grätzel and O'Reagan first proposed TiO_2-based dye-sensitized solar cells (DSSCs) with low costs and high photo-conversion efficiencies [1]. In recent years, one-dimensional TiO_2 nanotube arrays grown on Ti foils have attracted significant attention for use in dye-sensitized solar cells, due to their enhanced capability in terms of light harvesting and electron transport [2–4]. However, the amount of dye adsorption and the electron–hole recombination rate are two major limitations to further improvement of the conversion efficiency of dye-sensitized solar cells that use TiO_2 nanotube arrays as the photo-anode. An efficient method for suppressing the charge recombination is to composite the nano-semiconductor with wide band gap metal oxides, such as ZnO [5,6], MgO [7] or Al_2O_3 [8], which increase the physical separation of the injected electrons from the redox electrolyte, through the formation of an inherent energy barrier.

A heterojunction structure has the potential to reduce the chance of electron–hole recombination [9]. Composited nano-semiconductors can change their dimensions of the structure, which may be a combination of one-dimensional, two-dimensional or three-dimensional nanostructures, to improve surface area [10]. This method has been widely used in photo-catalysts but has rarely been reported for dye-sensitized solar cells, especially in modified one-dimensional TiO_2 nanotube arrays.

ZnO is one of the most widely studied multifunctional nano-semiconductors and is popular because of its wide band gap (3.37 eV) and large excitation binding energy (60 meV) [11]. The charge transfer for the heterojunction ZnO/TiO_2 process is depicted in Fig. 1 [12]. Efficient improvement in the conversion efficiency of

* Corresponding author. Tel.: +886 73814526x5116; fax: +886 73830674.
** Corresponding author.
E-mail addresses: ywd@cc.kuas.edu.tw (W.-D. Yang), qiangls@sina.com (L.-S. Qiang).

0378-7753/$ – see front matter © 2012 Elsevier B.V. All rights reserved.
http://dx.doi.org/10.1016/j.jpowsour.2012.07.097

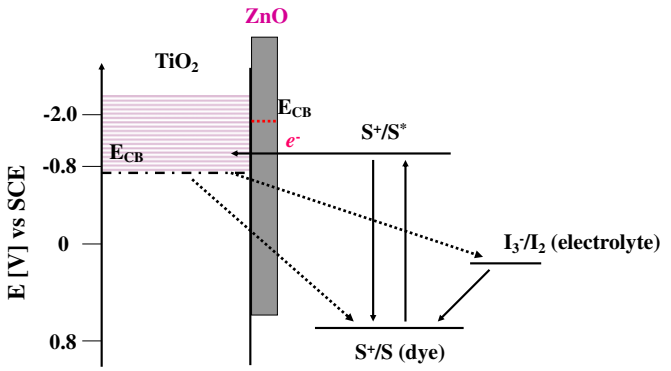

Fig. 1. Illustration of the interfacial charge transfer process occurred in the ZnO covered TiO_2/dye/electrolyte of dye-sensitized solar cells.

DSSCs depends on shortening the recombination pathway between the TiO_2, dye and the electrolyte, because an increased pathway provides a greater chance for electrons to recombine. A possible recombination route involved the reaction of the injected electrons with oxidized dye molecules. Another important reaction is the recombination of the oxidized redox couple. ZnO can form an inherent barrier layer between the electrode and the electrolyte interface, which increases the physical separation between the injected electrons and the oxidized dye redox couple and retards the electron recombination reaction. Kang et al. [13] coated the ZnO shell on the TiO_2 nanotube to improve the open-circuit voltage and conversion efficiency of the solar cells, mainly because a ZnO shell coated on the TiO_2 nanotubes forms recombination barrier. Qiu et al. [14] introduced a template-assisted process to assemble the TiO_2 coating on ZnO nanorods with a result of improvement in conversion efficiency. Kim et al. [15] used ZnO powders covered TiO_2 electrodes to enhance the performance of dye-sensitized solar cells, which improved both the short-circuit photocurrent and the open-circuit voltage. Pang et al. [16] researched the effect of different sizes of ZnO nanorods on the efficiency of TiO_2-based dye-sensitized solar cells and the effects of different amounts of ZnO on the charge-carrier transport. The experimental results showed that ZnO nanorods can improve charge transport, decrease recombination, enhance V_{oc} and increase conversion efficiency.

In this work, a ZnO semiconductor was used to modify the surface of anodic TiO_2 nanotubes, as the photo-anode of dye-sensitized solar cells using a convenient electrochemical deposition technique. The effects of different ZnO deposition times on dye-sensitized solar cells were also investigated.

2. Experimental procedure

The detailed fabrication process for the TiO_2 nanotube arrays is presented in a previous publication [17]. In this experiment, the electrolyte was 0.5 wt% NH_4F, glycerol and water (v:v = 2:1), the voltage was 30 V and the anodization time was 12 h. The TiO_2 nanotubes were heated at 500 °C for 2 h (heating and cooling rate were both 10 °C min^{-1}).

The three-electrode system was used to cause cathodic electrodeposition of ZnO on highly ordered TiO_2 nanotubes. The TiO_2 nanotubes are the working electrode, a saturated calomel electrode and a platinum electrode served as the reference and counter electrodes, respectively. The electrolyte contained 0.01 M $ZnAc_2$, 0.1 M KCl and 0.005 M H_2O_2. The cathodic potentials were fixed at −1.3 V, with deposition times ranging from 15 min to 120 min, at 70 °C. After deposition, the samples were calcined at 380 °C for 2 h (heating and cooling rate were both 10 °C min^{-1}). The prepared sample was marked as ZnO/TiO_2.

The dye-sensitized solar cells were assembled as follows: the as-prepared TiO_2 nanotubes and different amounts of ZnO/TiO_2 nanotubes were soaked in 0.3 mM solutions of *cis*-$RuL_2(SCN)_2$ (L = 2,2′-bipyridyl-4,4′-dicarboxylic acid) dye (N3 dye) for 24 h at 70 °C and then rinsed in ethanol to remove nonchemisorbed dye, where they were dried in an oven. The platinum counter electrode was prepared by spin-coating 5 mM H_2PtCl_6 (in ethanol) onto the FTO glass. It was then calcined at 385 °C for 10 min. A hot melt polymer (Solaronix SX1170-25, 60 μm) was used as an adhesive spacer. The ionic liquid electrolyte included 0.1 M LiI, 0.05 M I_2 and 0.5 M 4-tert-butylpyridine (TBP) in acetonitrile. The electrolyte was injected between two electrodes and driven by capillary force through holes on the hot melt sealing foil in the glove box. The TiO_2 films and the counter electrode were spaced and sealed by hot melt film as a spacer like a sandwich. The schematic diagram of configuration of the DSSCs is shown in Fig. 2.

XRD patterns were obtained by X-ray diffraction (XRD, PANalytical/X'Pert PRO MPD), using Cu Kα (λ = 0.154 nm) radiation at 10 kV and 100 mA; the samples were scanned from 20° to 80°. Field-emission scanning electron microscopy (FESEM, JEOL JSM-7401F) at 5 kV and the transmission electron microscopy (TEM, Philips: CM-200 TWIN) were used to observe the morphologies of the electrolytes. The UV–vis DRS spectra (Perkin Elmer; Lambda 35) of samples were measured from the optical absorption spectra, using a UV–vis spectrophotometer. X-ray photoelectron spectroscopy (XPS, Kratos Axis Ultra DLD) patterns were obtained using a monochromatic Al-anode X-ray gun. Photocurrent–voltage characteristics were measured under simulated solar light (AM-1.5, 100 mW cm^{-2}) using a Keithley 2400 sourcemeter; the active area of the solar cells was 0.25 cm^2. Electrochemical impedance spectra (EIS) were measured at open-circuit voltage, with a bias of 10 mV for frequencies from 10^{-1} to 10^5 Hz, to analyze the electron transport properties. An appropriate equivalent circuit model was used to fit the impedance spectra of the TiO_2 nanotubes photo-anode using ZsimpWin software.

3. Results and discussions

Fig. 3 shows a typical FESEM image of the anodic TiO_2 nanotube arrays. The average inner diameter of the TiO_2 nanotube arrays is 83 nm (Fig. 3(a)) and the average tube length is approximately 14 μm (Fig. 3(b)). The pores are uniform and highly ordered. The inset of Fig. 3(b) shows a magnified cross-sectional image, which shows that the structure of tube walls is similar to bamboo. After 15 min of ZnO cathodic deposition on the TiO_2 nanotubes, as shown

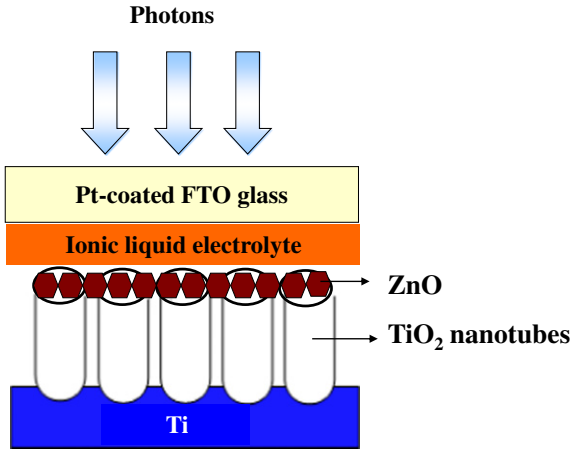

Fig. 2. Schematic illustration of the fabrication of dye-sensitized solar cells.

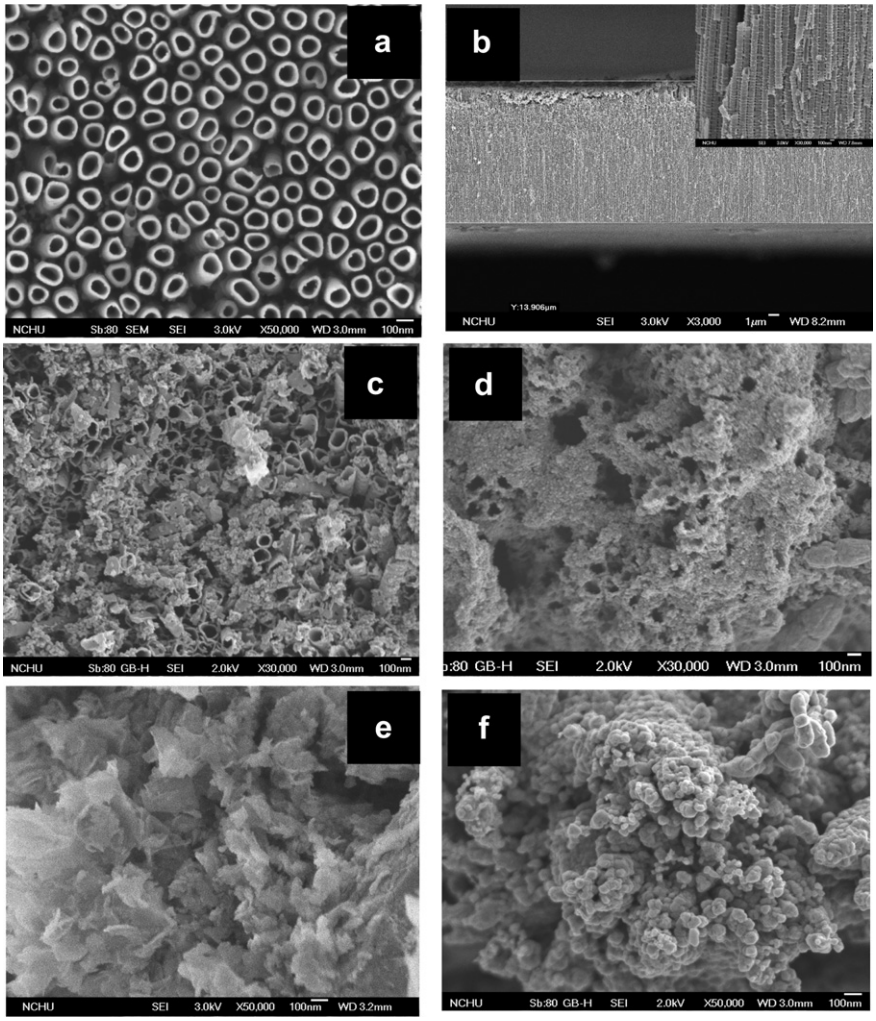

Fig. 3. FESEM images of TiO_2 nanotube arrays and ZnO/TiO_2 nanocomposites with different deposition times: (a) top and (b) cross-sectional views of TiO_2 nanotubes, (c) ZnO/TiO_2 (15 min), (d) ZnO/TiO_2 (30 min), (e) ZnO/TiO_2 (60 min) and (f) ZnO/TiO_2 (120 min).

in Fig. 3(c), ZnO grows non-uniform through inner channel of TiO_2 nanotubes. Fig. 3(d) represents more amount of ZnO grow on the TiO_2 nanotubes for 30 min deposition. Fig. 3(e) shows the image of ZnO/TiO_2 after 60 min of cathodic deposition. ZnO spilled from inner channel to the surface of the TiO_2 nanotubes, which is high in density and uniform. When deposition time was 120 min, a fairly thick agglomeration of ZnO occurs on the surface of TiO_2 nanotubes.

Fig. 4 shows the XRD patterns of the TiO_2 nanotubes and ZnO/TiO_2 nanocomposites. Fig. 4(a) shows the peak values of 25.28°and 48.04°, which are attributed to the crystal planes (101) and (200) of the anatase phase, the other peaks come from the titanium substrate. When deposition time is 15 min, the characteristic diffraction peaks of ZnO have not obviously appeared, which may be due to the presence too little ZnO to allow observation of diffraction peaks. In addition, ZnO/TiO_2 (15 min) also exhibits the characteristic anatase diffraction peaks of TiO_2 nanotubes. Based on the values of the ZnO standard card, after 30 min deposition, ZnO/TiO_2 composites show not only the characteristic anatase diffraction peaks, but also new peaks with values of 31.9°, 34.5°, 36.3° and 56.6°, which can be exactly ascribed to the hexagonal crystal structure of ZnO. The characteristic peaks of ZnO increases with increasing deposition time. Moreover, as deposition time increases to 2 h, the anatase (101) peak decreases, which indicate a thick ZnO

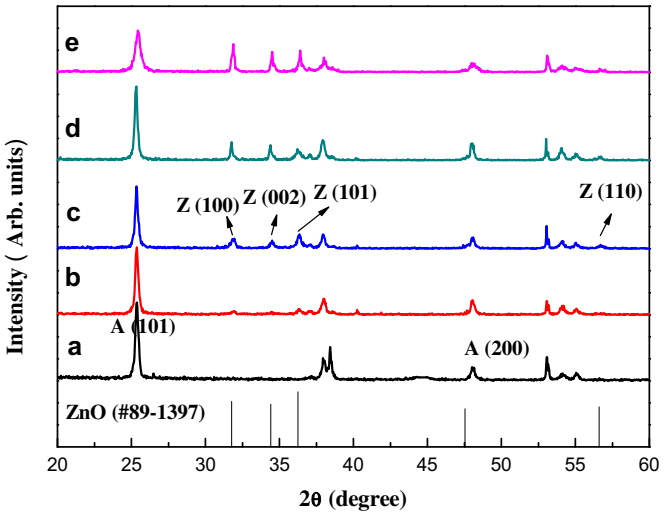

Fig. 4. XRD patterns of (a) TiO_2 nanotube arrays, (b) ZnO/TiO_2 (15 min), (c) ZnO/TiO_2 (30 min), (d) ZnO/TiO_2 (60 min) and (e) ZnO/TiO_2 (120 min).

film that affects observation of the TiO_2 crystal phase. These findings imply that the ZnO/TiO_2 composites possess anatase crystal TiO_2 and hexagonal wurtzite ZnO.

The TEM image of the ZnO/TiO_2 composites (1 h deposition) is shown in Fig. 5(A). The tubular structure and some additional materials can be observed. These materials were confirmed by electron diffraction spectroscopy (EDS), as shown in Fig. 5(C). The elemental compositions are Ti, O and Zn. Fig. 5(B) shows the HR-TEM image of the ZnO/TiO_2 structure, which shows clear lattice spacing of the crystal plane. It can be seen that ZnO (100) and TiO_2 (101) crystal plane are also observed, which are consistent with the XRD analysis. The red dotted line represents the boundary between the TiO_2 and ZnO. The inset picture in Fig. 5(B) is the selective area electron diffraction analysis, which confirms the TiO_2 nanotubes are anatase.

Fig. 6(A) shows the diffuse reflectance UV–vis spectroscopy of the TiO_2 nanotubes and ZnO/TiO_2 nanocomposites with a wavelength range of 300–800 nm. There is an obvious red shift compared with TiO_2 nanotubes, possibly due to differences in the surface state of the ZnO/TiO_2 composites. In addition, the absorbance of spectra increases, as deposition time increases, due to the increased amount of ZnO. To obtain the band gap, the spectrum shown in Fig. 6(A) was replotted in Fig. 6(B). The theory of optical absorption defines the relationship between the absorption coefficient and the photoenergy. The relevant equation for a direct transition semiconductor is shown as follows [18]: $\alpha = (h\upsilon - E_g)^{0.5}/h\upsilon$, Here, $\alpha = A/t$, where α is a coefficient, A is absorbance, t is film thickness and $h\upsilon$ is photo energy. Using this equation, curves of $h\upsilon$ used versus $(\alpha h\upsilon)^2$ were plotted and given the extrapolated liner portion corresponding to the E_g value. The estimated band gap energy was 3.19 eV for TiO_2 nanotubes and 3.14, 3.09, 2.94, 2.93 eV for ZnO/TiO_2 with deposition time of 15 min, 30 min, 60 min and 120 min, respectively. To the author's best knowledge, the band energy of ZnO is 3.37 eV and that for anatase TiO_2 is 3.20 eV. The band energy of ZnO/TiO_2 composites is lower than that for ZnO and TiO_2 nanotubes. That is because the presence of ZnO can modify the optical properties, to extend the range of the excited spectrum and favor the absorption of solar energy in the visible region. It also has been found that a red shift occurs, as ZnO deposition time increased, causing an increase on the amount of Zn.

The chemical components and chemical changes due to the modification of the amount of ZnO on the surface of TiO_2 nanotubes were examined by XPS, as shown in Fig. 7. ZnO/TiO_2 nanocomposites with a 1 h deposition time were selected to analyze changes of surface state. Fig. 7(A) shows the spectra of TiO_2 nanotubes and ZnO/TiO_2 composites over the wide scan range. Zn was observed for the composites, because of the ZnO coating on the TiO_2 nanotubes. High resolution XPS spectra of the Zn on the surface of ZnO/TiO_2 composites are shown in Fig. 7(B). The Zn $2p_{3/2}$ peak at approximately 1021.6 eV is assigned to the Zn–O bonds [19], which indicate the formation of a ZnO covering on the surface of TiO_2 nanotubes by electrochemical deposition.

The narrow scans of the Ti 2p peaks for the TiO_2 nanotubes and the ZnO/TiO_2 composites are shown in Fig. 7(C). A slight shoulder peak is observed at approximately 459.8 eV. This is due to the formation of Ti^{3+}. The strong chemical activity of Ti^{3+} can transfer excessive electrons to the carboxylate group of the dye molecules, which forms coordination bonding and may increase the amount of dye adsorption [14]. Moreover, the formation of Ti^{3+} can increase oxygen vacancies, which support the transport of electrons and holes between dye molecules and the photo-anode. The Ti (2p) peak of ZnO/TiO_2 composites shift to a lower banding energy. It also shows that coated ZnO can change the energy band of TiO_2. In Fig. 7(D), it can be seen that a good symmetric O 1s peak was obtained for pure TiO_2 nanotubes, while O 1s peak for ZnO/TiO_2 composites is asymmetric. Software (XPSPeak 41) can separate the asymmetric peak and reveal a main peak at 529.7 eV and an additional peak at 531.9 eV, as seen in Fig. 7(D) inset, which are respectively ascribed to the oxygen atoms of TiO_2 and ZnO [20].

Fig. 8 shows cyclic voltammogram (C–V) curves for the pure TiO_2 nanotubes and ZnO/TiO_2 composites with different deposition times, at a scan rate of 100 mV s^{-1} and the potential ranging from 0 V to 0.9 V in 1 M NaOH solution, in which the scales of right Y-axis is corresponding to the value of bare TiO_2 nanotubes and the scales of left Y-axis is related to the values of ZnO/TiO_2 composites with different deposition times. C–V measurements reveal interfacial electron flow in the TiO_2/electrolyte. The pronounced oxidative peak was observed during cyclic scans, while no obvious reactive wave is evident, suggesting a poorly reversible redox reaction. Bare TiO_2 nanotubes have a low current response, while the highest current occurs for a ZnO deposition time of 1 h, which indicates that ZnO-coated TiO_2 nanotubes show an improvement in charge transfer through the trap/surface states in the TiO_2 band gap. As XPS analysis shows, the formation of Ti^{3+} in ZnO/TiO_2 composites is beneficial to electron transfer. However, ZnO/TiO_2 composites with a deposition time of 1 h have a lower potential of approximately 0.3 eV, which indicates that the formation of a ZnO blocking barrier can suppress electron flow in the electrolyte. As previous noted, the addition of ZnO significantly influences the electron lifetime and electron transfer and result in an improvement in V_{oc} for the solar cells.

To determine the amounts of dye absorption, UV–vis spectroscopy measurements were performed on the desorbed dyes. The dyes were desorbed from dye-coated electrodes into 0.1 M KOH for 15 min. Using Beer's law, the dye loading can be calculated by fitting the absorption at 510 nm to the calibration curve. The amounts of dye are shown in Table 1. For bare TiO_2 nanotubes, the dye loading is 6.56×10^{-8} mol cm^{-2}. The amount of dye adsorption increases with increasing deposition time of ZnO. That is because the heterojunction ZnO/TiO_2 is a combination of one-dimensional, two-dimensional and three-dimensional nanostructures, which may provide more chance to absorb dye. On the other hand, the heterojunction ZnO/TiO_2 maybe exhibit a greater hydrophilicity. This probably occurs because of the presence of Ti^{4+}/dye and the formation of Zn^{2+}/dye complexes, which results in a greater

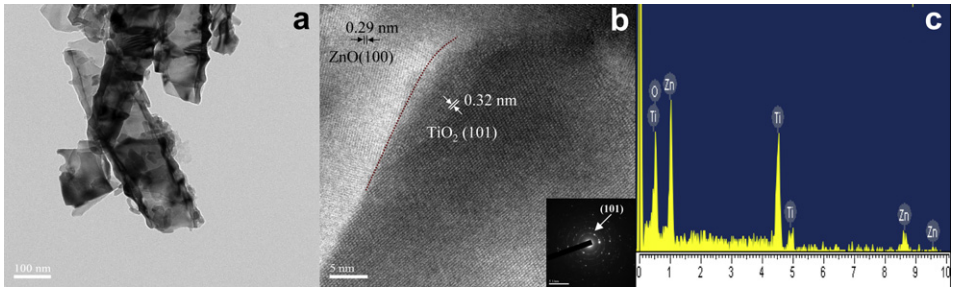

Fig. 5. TEM images of the ZnO/TiO_2 (60 min) nanocomposites: (A) low-magnification TEM image, (B) HR-TEM images and (C) EDS element images.

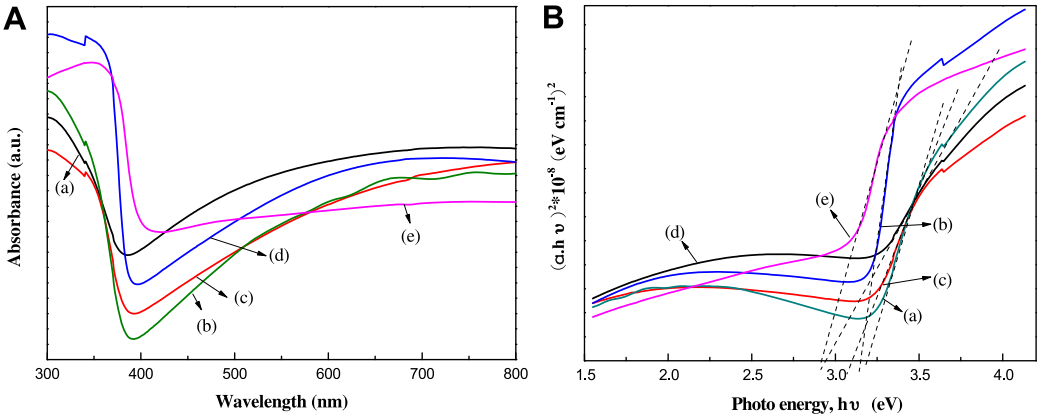

Fig. 6. (A) UV–vis RDS spectra and (B) the optical absorption edges (eV): (a) TiO_2 nanotube arrays, (b) ZnO/TiO_2 (15 min), (c) ZnO/TiO_2 (30 min), (d) ZnO/TiO_2 (60 min) and (e) ZnO/TiO_2 (120 min).

absorption of dye molecules. The highest amounts of dye absorption were achieved for 60 min deposition. However, the amount of dye absorption was decreased to 9.38×10^{-8} mol cm^{-2} when ZnO deposition 120 min, which is probably attributable to a large number of ZnO agglomerations on the surface of the TiO_2 nanotubes, as verified by SEM observation. Too thick ZnO film may be keep some dyes out TiO_2 nanotubes.

Fig. 9 shows the effect on the *I–V* characteristics of DSSCs of different electrochemical deposition times for the TiO_2 nanotubes and ZnO/TiO_2 composites. The corresponding values are summarized in Table 1. For bare TiO_2 nanotubes, the DSSCs have a J_{sc} value of 3.944 mA cm^{-2}, a V_{oc} value of 0.755 V and a fill factor (FF) of 0.567, giving an overall conversion efficiency of 1.710%. When ZnO is coated on the TiO_2 nanotube arrays for 15 min, the conversion efficiency of the DSSCs is 2.632%, with a J_{sc} of 4.652 mA cm^{-2}, a V_{oc} of 0.851 V and an FF of 0.665. As can be seen, the J_{sc} value was increased, suggesting that the presence of ZnO allows high dye adsorption, as shown in Table 1. As a result, light harvesting is improved. The increased V_{oc} may be due to the formation of a thin blocking layer of ZnO on the surface of TiO_2 nanotubes, which suppresses charge recombination between the photoinjected electrons of TiO_2 and I_3^- of the redox electrolyte, and also increases electron transport. Moreover, deposition of ZnO onto the TiO_2 nanotubes can move the TiO_2 conduction band in a negative direction, as confirmed by *C–V* analysis, which forms an inherent barrier layer that retards charge recombination and results in an improved V_{oc}.

The fill factor, which is related to internal resistance, is also an important factor for improvement of the efficiency of DSSCs. Of the

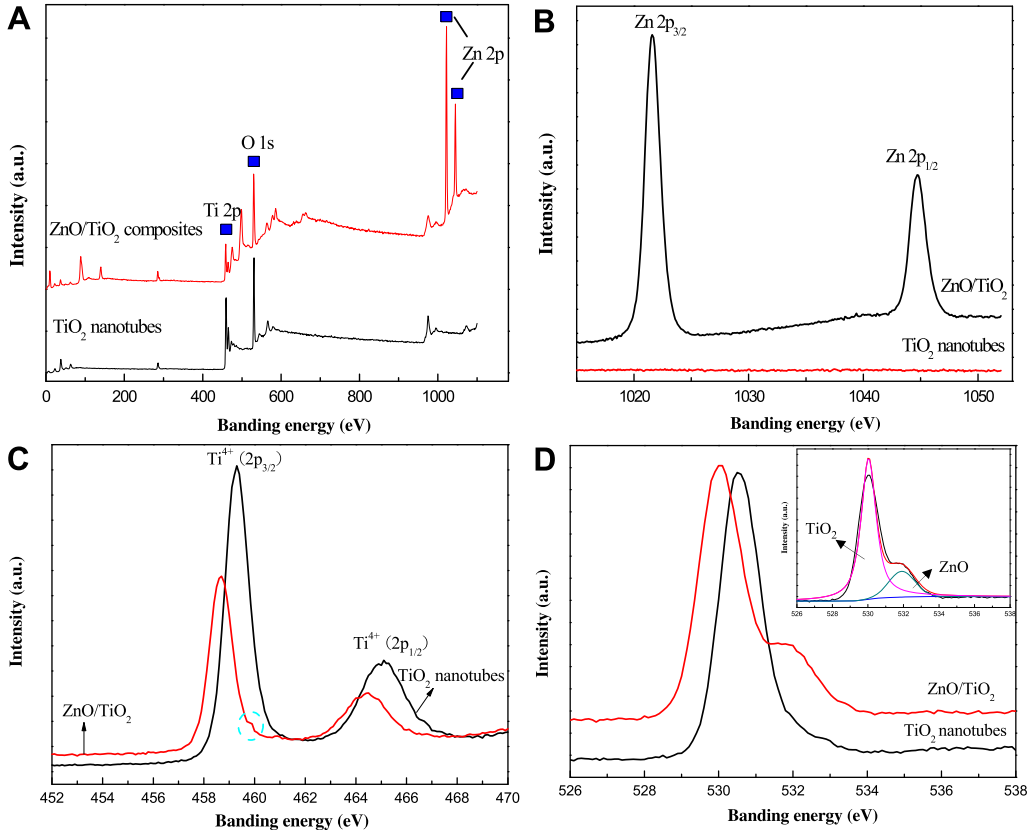

Fig. 7. XPS of bare TiO_2 and the ZnO/TiO_2 (60 min) nanocomposites in (A) the wide scan range, (B) the Zn 2p level peak, (C) the Ti 2p level peak and (D) the O 1s core level peak.

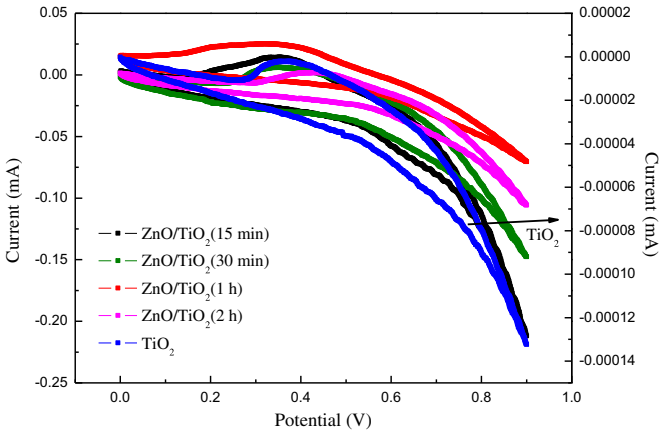

Fig. 8. Cyclic voltammograms of the bare TiO_2 nanotubes and ZnO/TiO_2 nanocomposites with different deposition times.

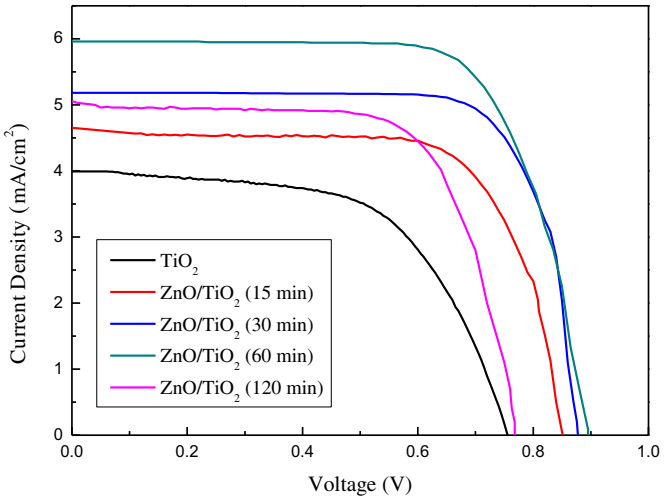

Fig. 9. Photocurrent–voltage (I–V) characteristic of dye-sensitized TiO_2 nanotubes and ZnO/TiO_2 nanocomposites solar cells with different deposition times.

series resistance is decreased, the fill factor is increased. A proper thin barrier layer can lead to a reduction in resistance, as explained by EIS analysis. An increase in the ZnO deposition time increases the J_{sc}, V_{oc} and FF. In comparison, for the highest efficiency, observed for DSSCs fabricated with a ZnO deposition time of 60 min, the J_{sc} is 5.960 mA cm^{-2}, V_{oc} is 0.895 V and FF is 0.704, which gives an efficiency of 3.755%, namely more than double the conversion efficiency of bare TiO_2 nanotube arrays. However, the conversion efficiency decreases, as ZnO deposition time increased to 120 min. A low efficiency is 2.608%, with a J_{sc} of 5.060 mA cm^{-2}, a V_{oc} of 0.768 V and an FF of 0.671. One possible reason is that too much ZnO surround the trap sites and hinder electron transport, which implies injection of excited electrons into the TiO_2 conduction band is inhibited. Another explanation is that the film on the TiO_2 nanotubes may be destroyed after the addition of such a large amount of ZnO, which affects the whole structure of electron transport. The decreased V_{oc} is mainly due to the presence of additional charge recombination sites.

The electron lifetime (τ) and electron transport were determined by electrochemical impedance spectroscopy (EIS). Bode plots and Nyquist plots are shown in Fig. 10(a) and (b) for various ZnO deposition times and bare TiO_2 nanotube arrays, respectively. Generally, there are three frequency peaks—low (in the range of mHz), medium (in the range at 1–1000 Hz) and high (in the range of kHz) frequency peak. The electron transport in TiO_2 nanotubes and charge reaction at the TiO_2/electrolyte interface are reflected in the medium frequency [21]. The corresponding characteristic mid-frequency peak (f_{max}) for TiO_2 nanotubes, 15 min, 30 min, 60 min and 120 min deposited ZnO/TiO_2 composites are located at 9.67 Hz, 8.11 Hz, 2.55 Hz, 1.91 Hz, 9.50 Hz respectively, as shown in Fig. 10(A). The electron lifetime can be estimated by the medium frequency using Eq. (2) [22]: $\tau = 1/2\pi f_{max}$, The corresponding values are also summarized in Table 1. Since the electron lifetime is related to electron recombination, the electron lifetime of ZnO/TiO_2 composites is obviously extended, which indicates the composites can efficiently suppress electron–hole recombination. There are two possible reasons for this. ZnO can form an energy barrier that can reduce the electron transfer from the TiO_2 conduction band to the I_3^- in the electrolyte, and increase V_{oc} [23]. Alternatively, TiO_2 and ZnO may form a heterojunction structure that reduces the electron concentration at the surface. A detailed investigation of the effect of the amount ZnO amount on the electron lifetime was also performed. The electron lifetime increased, as deposition time increased with a ZnO deposition time of 60 min yielding the longest lifetime, which implies the optimum film thickness can reduce the rate of recombination. Moreover, ZnO can trap the hole as following reaction [5]: $ZnO + 2h^+ \rightarrow Zn^{2+} + 1/2O_2$, where a large number electron merges in the conduction band of the TiO_2 nanotubes. Enrichment electrons can increase the potential between Fermi energy of TiO_2 nanotubes and redox electrolyte that reduces the recombination rate. For a deposition time of 120 min, the thickness of the ZnO layer is more than the optimum value, which may produce more charge recombination sites, as the electron lifetime is related to V_{oc}.

The related values for electron transport in the semiconductor can be obtained form the Nyquist plot. Fig. 10(B) shows the Nyquist plots for EIS for various ZnO deposition times and bare TiO_2 nanotube arrays. In general, the charge transfer resistance at the oxide/electrolyte interface can be determined from the arc diameter for the intermediated frequency (1–1000 Hz). For ZnO/TiO_2 nanocomposites coated for 15 min, 30 min, 60 min and 120 min, the R_{ct} values are 101, 82, 80 and 93 Ω, respectively. These values are smaller than the value of 114 Ω for the TiO_2 nanotubes, which is attributed to an increase in the interface area, due to the presence of ZnO. The variation in charge transfer resistance is explained by the electron lifetime. As above mentioned, an increased in the fill factor is explained by the total series resistance. This resistance can be expressed as a sum of the different contributions [24]: $R_{total} = R_s + R_{Pt} + 1/3R_{ct} + R_D$, where R_s is the series resistance, R_{Pt} is the charge transfer resistance at the counter electrode, R_{ct} is the

Table 1
Photovoltaic performance of DSSCs under AM-1.5 illumination.

Photo-anode	Dye loading (mol cm^{-2})	τ (ms)	V_{oc} (V)	J_{sc} (mA cm^{-2})	Fill factor	η (%)
TiO_2 nanotubes	6.56×10^{-8}	16.5	0.755	3.944	0.567	1.710
ZnO/TiO_2 (15 min deposition)	9.20×10^{-8}	19.6	0.851	4.652	0.665	2.632
ZnO/TiO_2 (30 min deposition)	9.51×10^{-8}	62.4	0.877	5.181	0.694	3.153
ZnO/TiO_2 (60 min deposition)	10.24×10^{-8}	83.4	0.895	5.960	0.704	3.755
ZnO/TiO_2 (120 min deposition)	9.38×10^{-8}	16.8	0.768	5.060	0.671	2.608

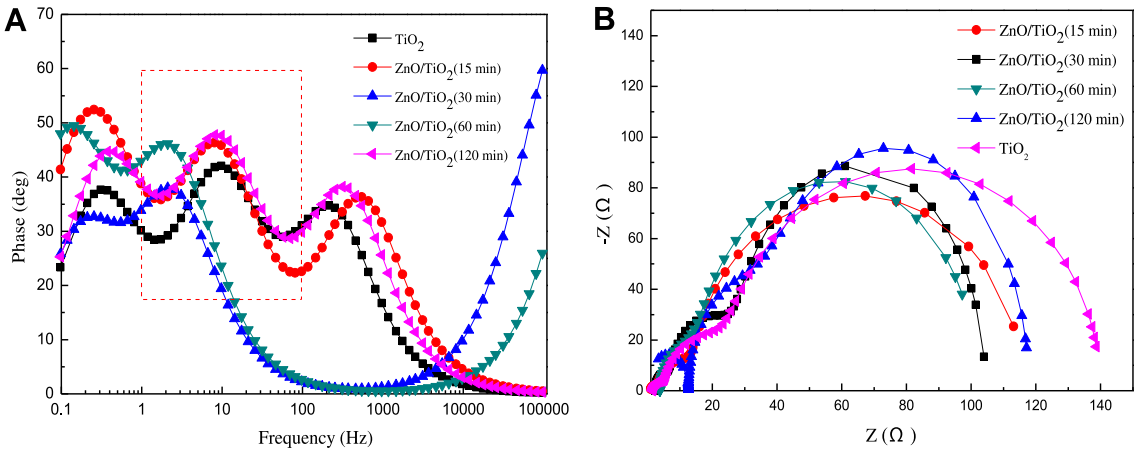

Fig. 10. Electrochemical impedance spectra of plain TiO_2 nanotubes and ZnO/TiO_2 nanocomposites with different deposition times: (A) Bode phase plots and (B) Nyquist plots.

charge transport resistance of the photo-anode and R_D is the direct current resistance for the diffusion of the redox species in the electrolyte. The values of R_s, R_{Pt} and R_D are considered to be equal, because these solar cells were fabricated under the same conditions, except for the use of a different photo-anode. The value of R_{ct} is the smallest for 60 min deposition, as a result of the favorable and effective electron transport at the interface. The lower total resistances of the TiO_2 nanotubes are contributed to the better fill factor value, as show in Table 1.

4. Conclusion

In summary, a convenient and effective technique was used to improve the efficiency of DSSCs. The surfaces of the TiO_2 nanotubes were modified with different amounts of ZnO using a simple cathodic electrodeposition method. The ZnO covered on the TiO_2 nanotubes exhibited a ZnO and TiO_2 crystal structure and lower band energy. As expected, the ZnO/TiO_2 nanocomposites have exhibited higher conversion efficiency of dye-sensitized solar cells. The highest conversion efficiency for ZnO deposition time of 60 min on TiO_2 nanotubes is more than double that for bare TiO_2 nanotubes. The changes in edge position and the suppression of charge recombination are the most important reasons for improvement V_{oc}. The higher dye adsorption and electron transfer contribute to the improvement in the photocurrent. It is also found that one-dimensional TiO_2 nanotubes are suitable for the fabrication of a heterojunction structure for dye-sensitized solar cells, which not only increase the dye loading, but also increase electron lifetime.

Acknowledgements

The authors would like to express their gratitude to the National Science Council of Taiwan for supporting this research under grant no. 100-2221-E-151-030.

References

[1] J.R. Jennings, A. Ghicovm, L.M. Peter, P. Schmuki, A.B. Walker, J. Am. Chem. Soc. 130 (2008) 13364–13372.
[2] M. paulose, G.K. Mor, O.K. Varghese, K. Shankar, C.A. Grimes, J. Photochem. Photobiol. A 178 (2006) 8–15.
[3] G.K. Mor, K. Shankar, M. Paulose, O.K. Varghese, C.A. Grimes, Nano Lett. 6 (2006) 215–218.
[4] J. Zhang, C.C. Tang, J.H. Bang, Electrochem. Commun. 12 (2010) 1124–1128.
[5] S.F. Chen, W. Zhao, W. Liu, S.J. Zhang, Appl. Surf. Sci. 255 (2008) 2478–2484.
[6] Z.H. Zhang, Y. Yuan, L.H. Liang, Y.X. Cheng, G.Y. Shi, L.T. Jin, J. Hazard. Mater. 158 (2008) 517–522.
[7] G.R.A. Kumara, M. Okuya, K. Murakami, J. Photochem. Photobiol. A 164 (2004) 183–185.
[8] H. Alarcon, G. Boschloo, P. Mendoza, J.L. Solis, A. Hagfeldt, J. Phys. Chem. B 109 (2005) 18483–18490.
[9] J.J. Yuan, H.D. Li, S.Y. Gao, Y.H. Lin, H.Y. Li, Chem. Commun. 46 (2010) 3119–3121.
[10] Q.F. Zhang, G.Z. Cao, J. Mater. Chem. 21 (2011) 6769–6774.
[11] L.S. Wang, M.W. Xiao, X.J. Huang, Y.D. Wu, J. Hazard. Mater. 161 (2009) 49–54.
[12] E. Palomares, J.N. Clifford, S.A. Haque, T. Lutz, J.R. Durrant, Chem. Commun. 14 (2002) 1464–1465.
[13] S.H. Kang, J.Y. Kim, Y.Y. Kim, H.S. Kim, Y.E. Sung, J. Phys. Chem. C 111 (2007) 9614–9623.
[14] J.J. Qiu, F.W. Zhuge, K. Lou, X.M. Li, X.D. Gao, X.Y. Gan, W.D. Yu, H.K. Kim, Y.H. Hwang, J. Mater. Chem. 21 (2011) 5062–5068.
[15] K.E. Kim, S.R. Jang, J. Park, R. Vittal, K.J. Kim, Sol. Energy Mater. Sol. Cells 91 (2007) 366–370.
[16] S. Pang, T.F. Xie, Y. Zhang, X. Wei, M. Yang, D.J. Wang, Z.L. Du, J. Phys. Chem. C 111 (2007) 18417–18422.
[17] R. Liu, W.D. Yang, L.S. Qiang, J.F. Wu, Thin Solid Films 519 (2011) 6459–6466.
[18] R.S. Mane, W.J. Lee, H.M. Pathan, S.H. Han, J. Phys. Chem. B 109 (2005) 24254–24259.
[19] S.S. Kim, J.H. Yum, Y.E. Sung, Photochem. Photobiol. A 171 (2005) 269–273.
[20] N. Wang, X.Y. Li, Y.X. Wang, Y. Hou, X.J. Zou, G.H. Chen, Mater. Lett. 62 (2008) 3691–3693.
[21] R. Kern, R. Sastrawan, J. Ferber, R. Stangl, J. Luther, Electrochim. Acta 47 (2002) 4213–4225.
[22] Q. Wang, J.E. Moser, M. Grätzel, J. Phys. Chem. B 109 (2005) 14945–14953.
[23] M.L. Wang, C.G. Huang, Y.G. Cao, Q.J. Yu, J. Phys. D: Appl. Phys. 42 (2009) 155104–155109.
[24] Q. Wang, S. Ito, M. Grätzel, F. Fabregat-Santiago, I. Mora-Seró, J. Bisquert, T. Bessho, H. Imai, J. Phys. Chem. B 110 (2006) 25210–25221.